## *Supplementary Information*

Morphology development studied by neutron reflectivity

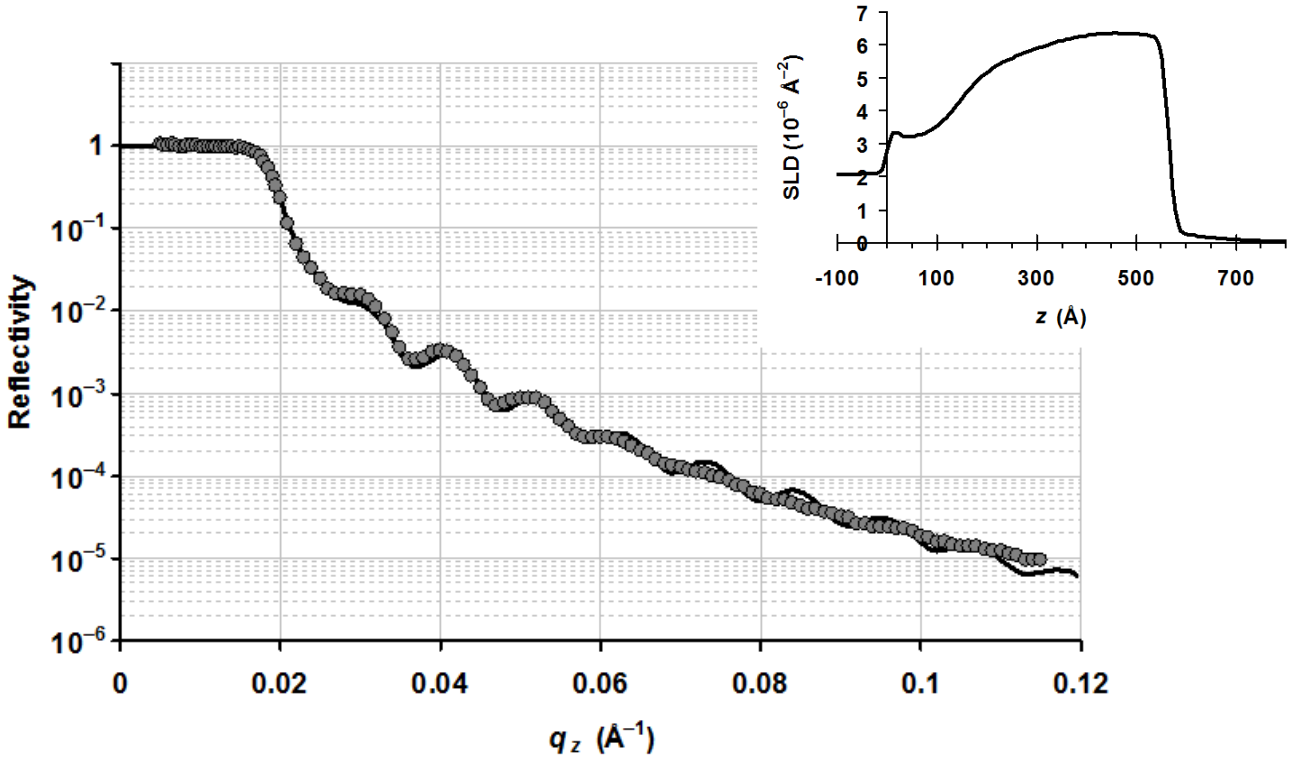


Figure S1: Neutron reflectivity for a film of deuterated polystyrene homopolymer (dPS), cast on the silica-nanoparticle roughened substrate. The solid line is a best-fit to the experimental data, with the associated scattering length density (SLD) profile shown inset. This control experiment highlights the height distribution of the rough substrate layer.

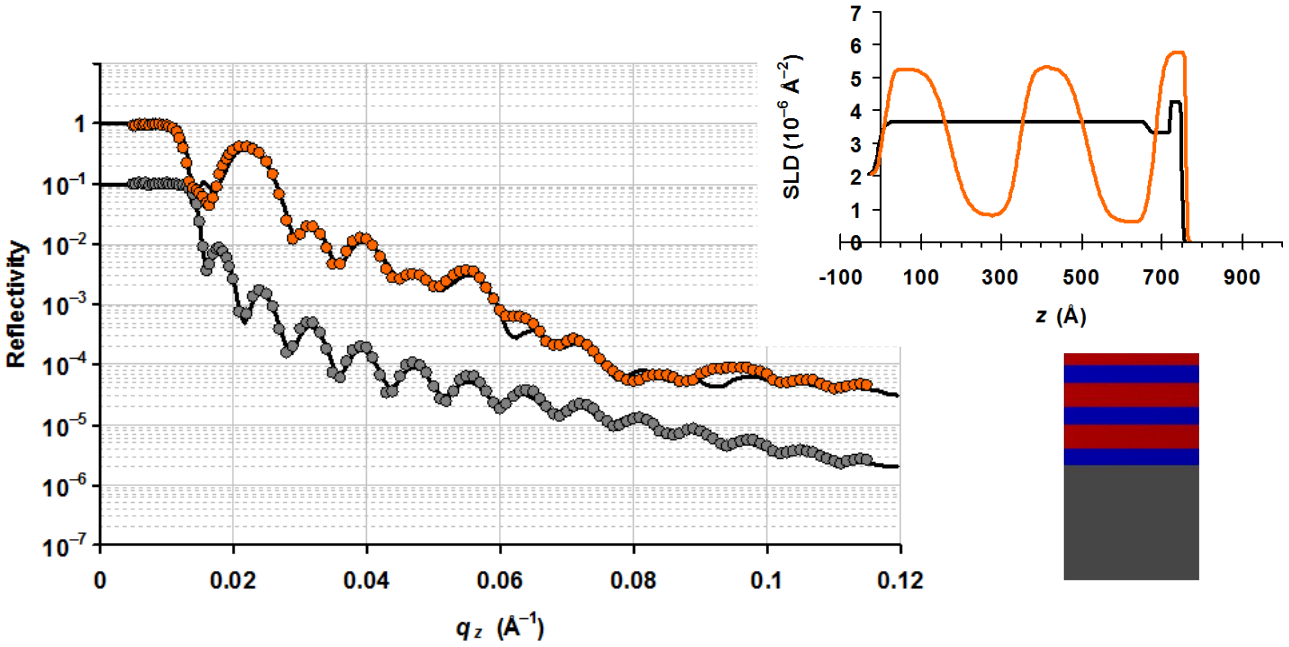


Figure S2: Neutron reflectivity for a film of dPS-PMMA block-copolymer cast on silicon wafer (with native oxide). The grey symbols are for the as-cast state; the orange symbols are after 4 hours annealing at 180 ºC. The solid lines are best-fits to the experimental data, with the associated scattering length density (SLD) profile shown inset. The initially disordered state forms horizontal lamellae after annealing.

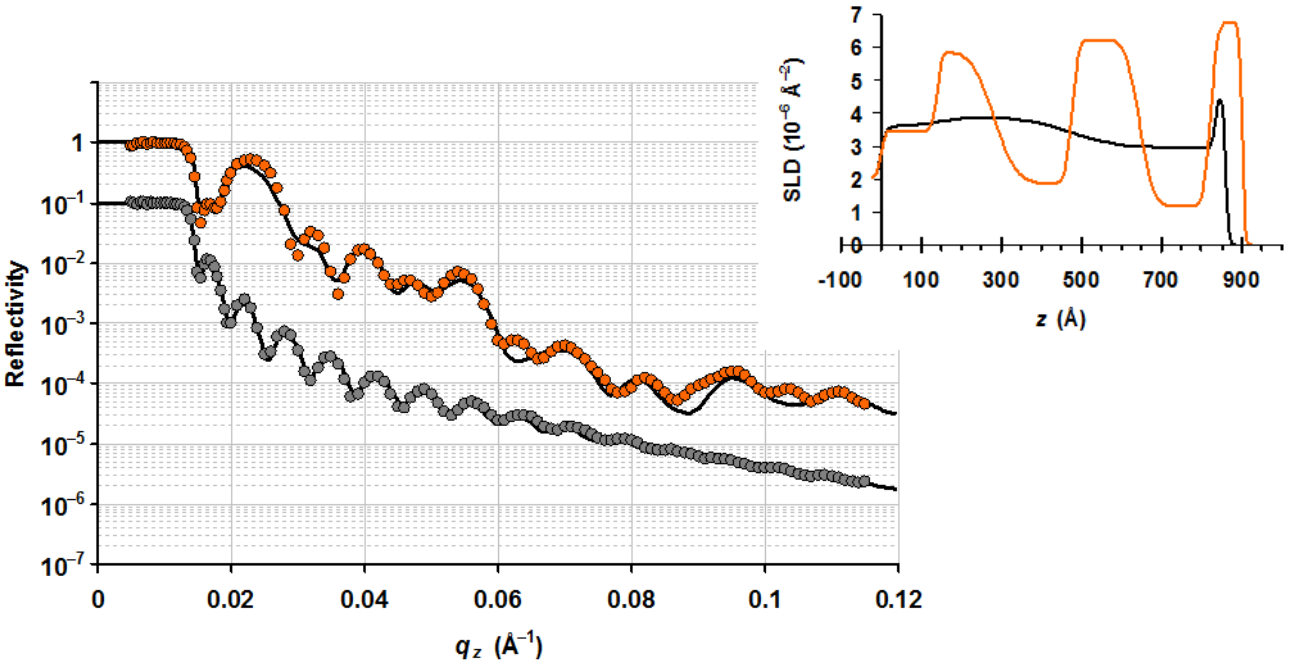


Figure S3: Neutron reflectivity for a film of dPS-PMMA block-copolymer cast on the silica-nanoparticle roughened substrate. Substrate was processed (see main text) to achieve a water contact angle of $\theta_w \approx 10^o$. The grey symbols are for the as-cast state; the orange symbols are after 4 hours annealing at 180 ºC. The solid lines are best-fits to the experimental data, with the associated scattering length density (SLD) profile shown inset. Although the final annealed state clearly exhibits a horizontal lamellae layering, the as-cast state does not show any discernible structure.

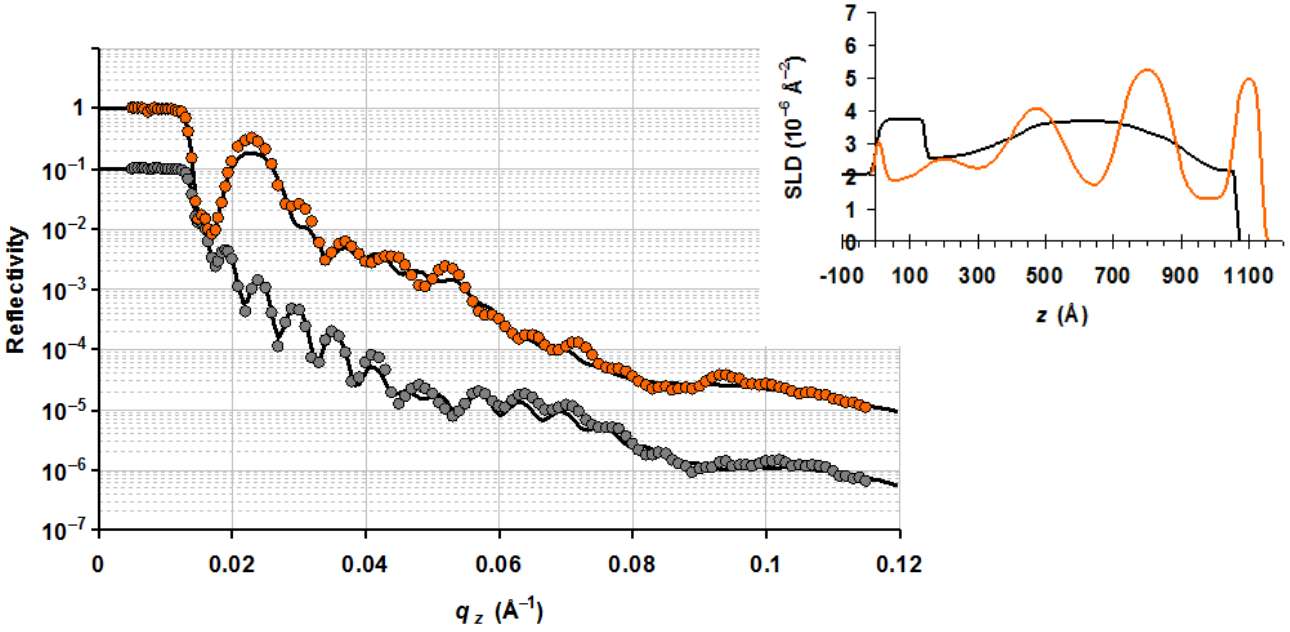


Figure S4: Neutron reflectivity for a film of dPS-PMMA block-copolymer cast on the silica-nanoparticle roughened substrate. Substrate was processed (see main text) to achieve a water contact angle of $\theta_w \approx 34^o$. The grey symbols are for the as-cast state; the orange symbols are after 4 hours annealing at 180 ºC. The solid lines are best-fits to the experimental data, with the associated scattering length density (SLD) profile shown inset. The final annealed state clearly exhibits a horizontal lamellae layering. The as-cast state exhibits weak segregation of BCP material, without a well-defined morphology.

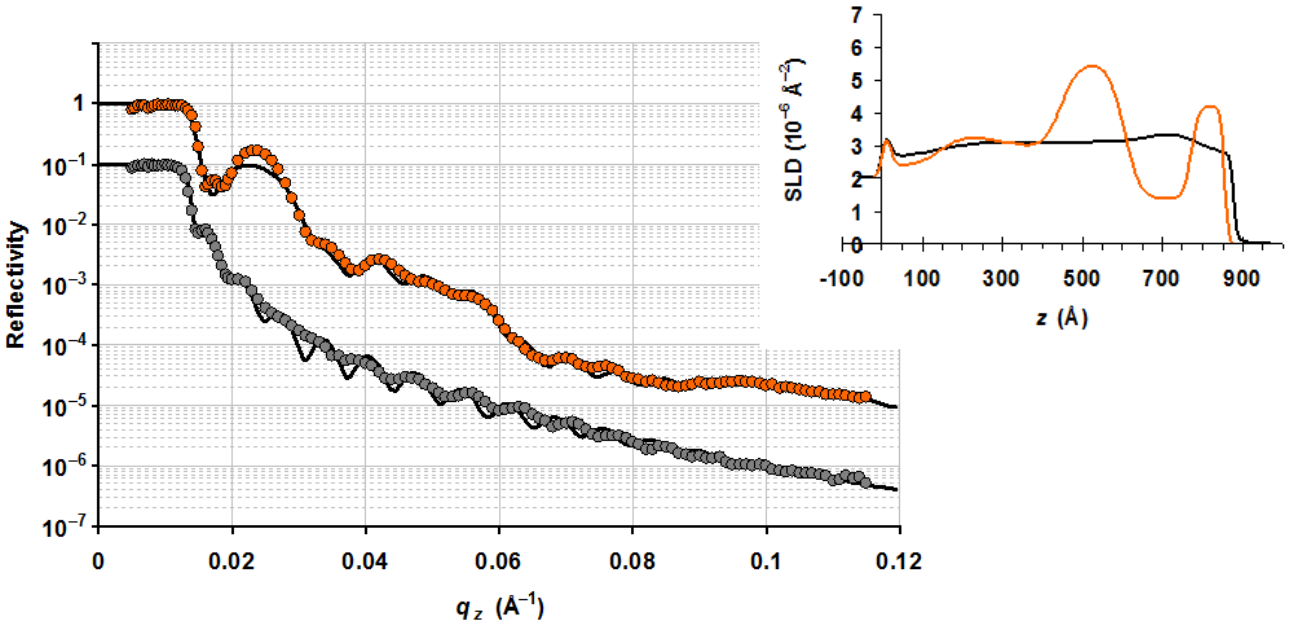


Figure S5: Neutron reflectivity for a film of dPS-PMMA block-copolymer cast on the silica-nanoparticle roughened substrate. Substrate was processed (see main text) to achieve a water contact angle of $\theta_w \approx 47^o$. The grey symbols are for the as-cast state; the orange symbols are after 4 hours annealing at 180 ºC. The solid lines are best-fits to the experimental data, with the associated scattering length density (SLD) profile shown inset. The final annealed state clearly exhibits a horizontal lamellae layering. The as-cast state exhibits weak segregation of BCP material, without a well-defined morphology.

Mixed orientation analysis

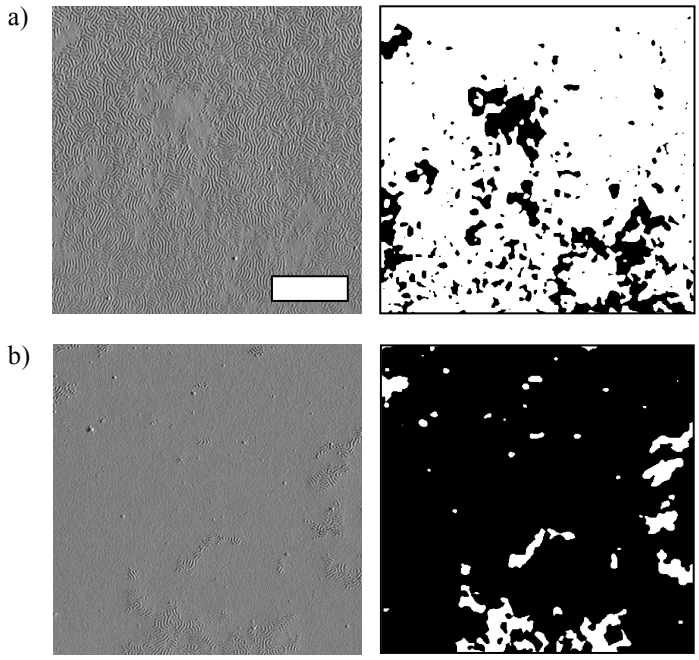


Figure S6: Typical AFM images (scale bar is 1 μm and applies to all images) of dPS-b-PMMA block-copolymer films annealed on nanoparticle-treated substrates. The images on the left are the phase-mode AFM data, and on the right are the corresponding segmentations, which divide the image into vertical regions (white) and horizontal regions (black). In a) the thin film thickness is 99 nm (4 h annealing at 165 ºC), which leads to a predominantly vertical morphology. In b) the film thickness is 84 nm, which leads to a predominantly horizontal morphology.

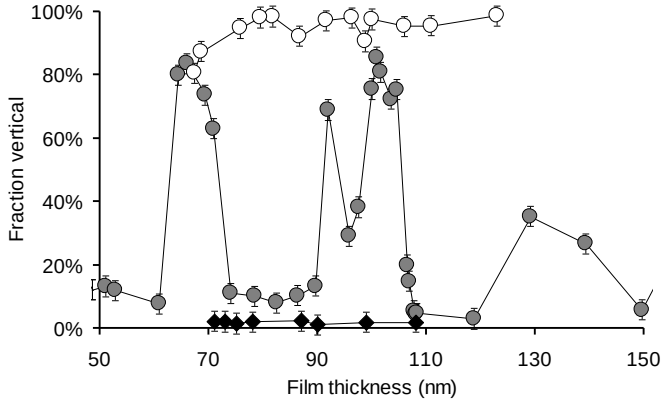


Figure S7: The fraction of film area exhibiting the vertical orientation (perpendicular lamellae), based on AFM image analysis. The open circles are for annealing at 150 ºC; the grey circles for 165 ºC; and the black diamonds for 180 ºC. The film is predominantly vertical at low-temperature, and predominantly horizontal at high-temperature. At 165 ºC, the surface morphology oscillates between predominantly vertical and predominantly horizontal, with a period equal to the domain spacing, $L_0$. Error bars were estimated from the standard deviation of repeated measurements at particular film positions. The connecting lines are guides to the eye only.

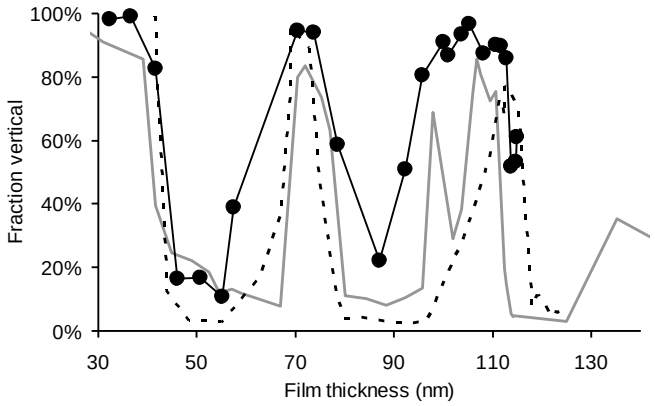


Figure S8: Effect of annealing time on surface morphology. After 4 h of annealing at 165 ºC (black connected circles), the film exhibits a preference for vertical morphology. After 18 h (grey curve), the film exhibits distinct oscillations between vertical and horizontal morphologies. After 20 h (dotted curve), this effect is somewhat more pronounced, with fewer 'vertical defects' in the horizontal regions. The oscillation between morphologies is stable even after extended annealing.

RSANS Analysis

The RSANS data can be analyzed quantitatively by fitting to a scattering model. Using the model of Ruland and Smarsly,[1] we separate the intensity into an angular distribution function, $g(\omega)$, and a one-dimensional scattering function ($I_1$) representing a 'stack' of lamellae:

$$I(q_x,\omega) \propto \frac{g(\omega)}{q_x^{\,2}} I_1(q_x) \tag{1}$$

We choose a distribution function of the form:

$$g(\omega) = \frac{A_v}{2\pi} \frac{1-s_v^{\,2}}{(1+s_v)^2 - 4s_v \cos^2 \omega} + A_h \frac{1-s_h^{\,2}}{(1+s_h)^2 - 4s_h \cos^2(\omega - \pi/2)} \tag{2}$$

where the $A_i$ represent the relative size of vertical ($v$) or horizontal ($h$) populations ($A_v + A_h = 1$), and the $s_i$ are order parameters describing the angular spread of the populations ($s_i = 0$ indicating an isotropic distribution, $s_i = 1$ indicating perfect alignment with no angular spread). The one-dimensional scattering function includes terms related to the Fourier transform of the lamellae interface distributions. In a lattice model:

$$I_1(q) = \frac{N(\rho_1 - \rho_2)^2}{2\pi^2 q^2} \left[ 1 - \mathrm{Re}\, H_1 + 2[\mathrm{Im}\, H_1(q/2)]^2 \left( \frac{|Z|^2}{N} - 1 \right) \right] \tag{3}$$

Where $N$ is the average number of lamellae in a stack, and $(\rho_1 - \rho_2)$ is the contrast in scattering density between the two blocks. For finite stacks, the distribution of the lamellae period is captured by:

$$\frac{|Z|^2}{N} = \mathrm{Re}\left[\frac{1+H_L}{1-H_L} - \frac{2H_L(1-\langle H_L^N \rangle}{N(1-H_L)^2}\right] \tag{4}$$

where the Fourier transform of the distribution of spacings, and its average over $N$, are given by:

$$\begin{aligned} H_1 &= \exp(2\pi i d_1 - 2\pi^2 \sigma_1{}^2 q^2) \\ H_L &= \exp(2\pi i L - 2\pi^2 \sigma_L{}^2 q^2) \\ \langle H_L^N \rangle &= \left[1 - \sigma_N{}^2 \ln(H_L)/N\right]^{-N^2/\sigma_N^2} \end{aligned} \tag{5}$$

Here, $L$ is the average lamellar period, $d_1 = L/2$ is the average width of the domains of component 1, and $\sigma_1$, $\sigma_L$, and $\sigma_N$ represent the spread of about the mean of the respective quantities. Because of the relatively poor resolution of SANS, we explicitly include resolution broadening in the model, following the treatment described by Pedersen *et al*.[2] The angular error (for the incident beam direction) is given by:

$$\Delta\beta \approx \frac{2r_1}{M} - \frac{1r_2{}^2}{2r_1}\frac{(m+M)^2}{m^2}\frac{1}{M} \tag{6}$$

where $r_1$ is the source aperture radius, $r_2$ is the sample aperture, $m$ is the source-sample distance, and $M$ is the sample-detector distance. Smearing also arises from wavelength spread and collimation error (detector errors were found to be negligible):

$$\sigma_W = \langle q \rangle \frac{\Delta\lambda}{\langle\lambda\rangle}\frac{1}{2\sqrt{2\ln 2}} \tag{7}$$

$$\sigma_C = \frac{2\pi}{\langle\lambda\rangle}\cos\langle\theta\rangle\frac{\Delta\beta}{2\sqrt{2\ln 2}} \tag{8}$$

For the present experimental conditions, the angular error (smearing in the $\omega$-direction) is relatively small ($\Delta\beta \approx 0.4°$), whereas the smearing in the $q$-direction is considerable (0.02 $\mathrm{nm}^{-1}$ to 0.04 $\mathrm{nm}^{-1}$). The experimental intensity maps were fit by minimizing the square residuals between the data and model maps. Because of the $q$-smearing and the use of relative (rather than absolute) intensities, the fit is

insensitive to some parameters ($\sigma_1$, $\sigma_L$, $\sigma_N$, $N$). The fit is however sensitive to the lamellae period ($L$), and the angular distribution ($A_v$, $s_v$, $A_h$, $s_h$), which are the primary variables of interest. The best-fits (shown in Figure 5 d–f) allow us to infer the angular distribution of lamellae for those samples, which is shown in Figure 6. This shows quantitatively the change in lamellae orientation as a function of thickness. At commensurate thicknesses, the horizontal component dominates ($A_h > A_v$), and is well-aligned ($s_h \approx 1$). At incommensurate thicknesses, this horizontal ordering is disrupted: the vertical fraction dominates ($A_v > A_h$), and the horizontal fraction is less ordered. In all cases, the vertical fraction is not perfectly aligned ($s_v \approx 0.4$) because it lacks the geometric constraint of the substrate interface. Nevertheless, the fits clearly show that at incommensurate thicknesses the lamellae preferentially align vertically (rather than isotropically), with a defined angular spread.

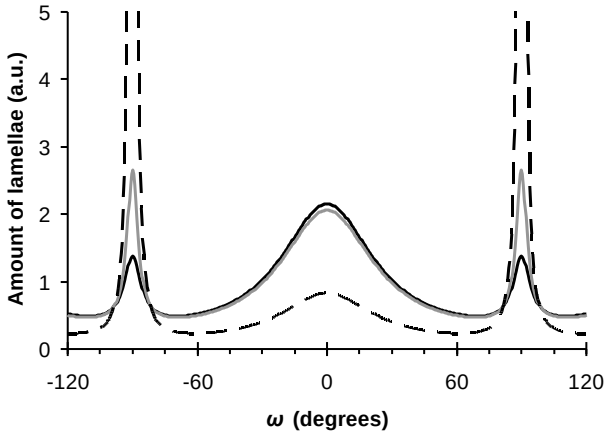


Figure S9: Inferred angular distribution of lamellae, based on the best-fits to the SANS data (Figure 3 in main text). The solid black curve is for the 78 nm film, which exhibits a large vertical fraction and small horizontal component ($A_v$ = 0.92, $s_v$= 0.40, $A_h$ = 0.08, $s_h$ = 0.85). The grey curve is for the 79 nm film, which exhibits a slightly increased horizontal component ($A_v$ = 0.88, $s_v$= 0.40, $A_h$ = 0.12, $s_h$ = 0.90). The dashed curve is for the 83 nm film, where the vertical component has nearly disappeared, and the horizontal component is large and well-ordered ($A_v$ = 0.35, $s_v$= 0.40, $A_h$ = 0.65, $s_h$ = 0.97).

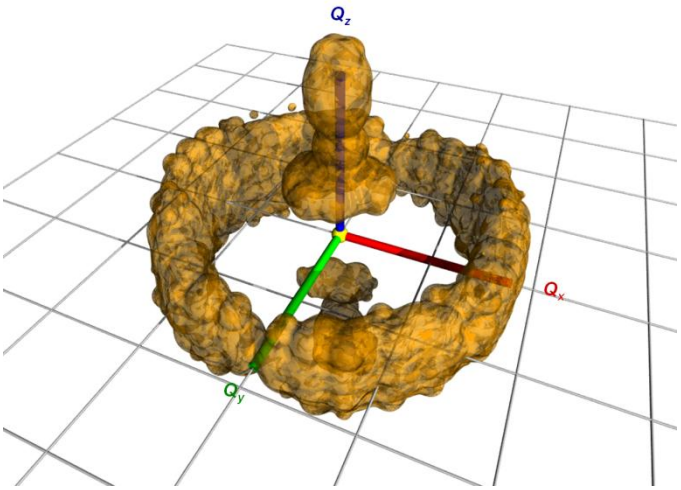


Figure S10: Example reciprocal-space intensity surface for a BCP thin film which exhibits a mixture of horizontal and vertical lamellae. The data is generated by accumulating SANS as a function of sample rotation angle. A surface of constant scattering intensity is plotted. The ring in the $Q_x$-$Q_y$ plane arises from the vertically-oriented lamellae (which have no preferred orientation in-plane). The lobes along the $Q_z$ axis arise from the horizontally-oriented lamellae.

## Surface Segregation

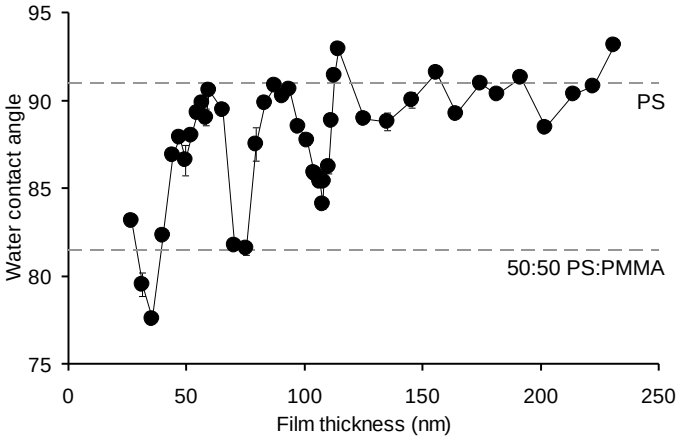


Figure S11: The water contact angle on the surface of a thickness gradient sample provides evidence for the surface chemistry. The oscillation in the contact angle data tracks the morphology oscillation, suggesting that in regions where the lamellae are oriented vertically, the morphology extends all the way to the free surface. The error bars, based on the standard deviation of replicates, are often smaller than the data points. The dashed lines denote the expected values for pure PS and for a mixture of PS and PMMA.

## Molecular Dynamics Simulation

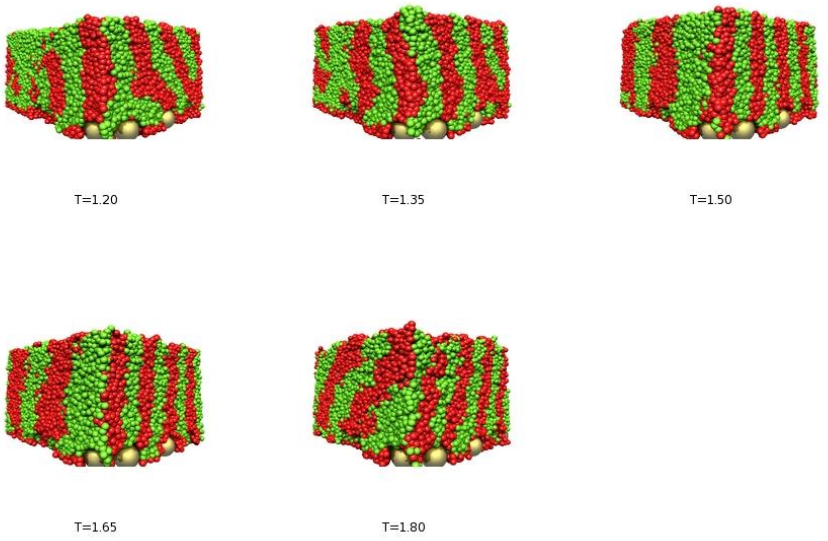


Figure S12: Final-state snapshots from molecular dynamics simulations of BCP lamellar films on rough substrates (see main text for simulation details). In this case, a nanoparticle surface coverage of ~50% (compared to the 35% used described for the main text results) was used. This large coverage gives rise to vertical lamellae at all temperatures probed.

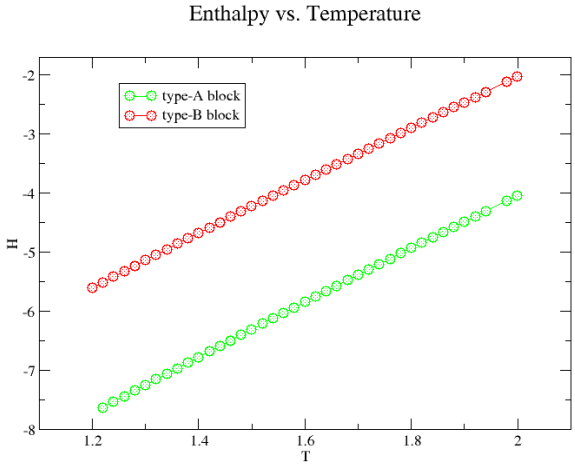


Figure S13: Enthalpy calculated for simulations run across a wide range of temperatures (in reduced simulation units). The glass-transition temperature of a polymer is marked by a kink in the response of volume and enthalpy with respect to temperature (i.e. a change in the linear-response). The linear response of enthalpy vs. temperature within the range probed confirms that these temperatures are above the glass-transition temperatures of both blocks.

## References

1. Ruland, W.; Smarsly, B., SAXS of self-assembled oriented lamellar nanocomposite films: an advanced method of evaluation. *Journal of Applied Crystallography* **2004,** *37* (4), 575-584.
2. Pedersen, J. S.; Posselt, D.; Mortensen, K., Analytical treatment of the resolution function for small-angle scattering. *Journal of Applied Crystallography* **1990,** *23* (4), 321-333.